Journal of Physics D: Applied Physics

ACCEPTED MANUSCRIPT

Biaxial strain induced strong enhancement of upconversion photoluminescence in lanthanide doped ferroelectric thin films

To cite this article before publication: Sisi Li *et al* 2019 *J. Phys. D: Appl. Phys.* in press https://doi.org/10.1088/1361-6463/ab08d1

Biaxial strain induced strong enhancement of upconversion photoluminescence in lanthanide doped ferroelectric thin films

Sisi Li,[a] Haisheng Chen,[b] Yanan Zhao,[b] Zhengwei Chen,[a] Er-jia Guo,[c] Zhenping Wu,[a,*] Yang Zhang,[b,d*] Weihua Tang,[a] Jianhua Hao,[e]

[a] *State Key Laboratory of Information Photonics and Optical Communications & School of Science, Beijing University of Posts and Telecommunications, Beijing 100876, China.*
[b]*Institute of Modern Optics, Nankai University, Tianjin, 300071, China*
[c]*Institute of Physics, China Academy of Science, Beijing, 100190, China*
[d]*Tianjin Key Laboratory of Optoelectronic Sensor and Sensing Network Technology, Tianjin, 300071, China*
[e]*Department of Applied Physics, The Hong Kong Polytechnic University, Hung Hom, Hong Kong, China*

Keywords: Biaxial strain engineering, Ferroelectric, Upconversion photoluminescence, Thin films, Lanthanide doped phosphors

* E-mail: zhenpingwu@bupt.edu.cn (Z. P. WU), yangzhang@nankai.edu.cn (Y. Zhang)

Abstract:

The ability to manipulate and enhance the optical properties in luminescent materials is of great interest for both scientific research and practical applications. Here we present a systematical study of the biaxial strain effect on the upconversion photoluminescence properties in the lanthanide doped ferroelectrics thin films. Through controlling the *c*/*a* ratios of $BaTiO_3$: Er films, the luminescent intensity of the films can be effectively increased by over 7 times. The observed phenomena can be understood by the crystal field variation around Er^{3+} ions induced by biaxial strain due to the lattice mismatch. Moreover, our results have bridged the identifications of lattice distortion and crystalline orientation through light emission properties of lanthanide dopants. The intriguing interplay will aid further design of favorable lanthanide doped phosphors via strain engineering.

1. Introduction

Lanthanide doped phosphors have stimulated intensive scientific interests for elucidating the potentially technological impact on modern information and optoelectronic devices.[1-6] No doubt, the ability of tuning the photoluminescence (PL) of these phosphors is particularly important for their applications.[7, 8] The optical properties of the lanthanide doped phosphors are determined by the doping ions as well as the host materials. To date, the manners for manipulating the PL of lanthanide doped phosphors fall into two basic categories, namely chemical and physical methods. The chemical method is generally achieved by changing the composition of doping ions and/or host materials.[9, 10] Owing to the abundant ladder-like arranged energy levels of the lanthanide ions, multicolor emissions can be obtained using different host/activator combinations.[11] However, the chemical method works in an irreversible and *ex-situ* manner, which makes it difficult to examine the pure crystal-field effect on the luminescent properties of doped lanthanide ions. Some kinds of smart materials, such as ferroelectrics and piezoelectrics can response to external stimuli, such as electric field, magnetic field, mechanical strain and temperature disturbance in a controlled manner.[12-22] In this regard, the physical approaches based on these materials promise the opportunities to tailor the PL process in an *in-situ* and real-time manner.[2] Our group had found that the upconversion PL of Yb^{3+} and Er^{3+} co-doped ferroelectric $BaTiO_3$ (BTO: Yb/Er) thin films can be effectively tuned by the electric field.[16] Later, Kwok and co-workers also reported that reversible modulation of PL in lanthanide doped ferroelectric ceramics could be attributed to electric-field-induced polarization

switching and phase transformation of the ceramics.[23] The variation in the crystal field of ferroelectric hosts exerts an essential influence on the luminescent active ions. According to the Judd-Ofelt theory, variable local symmetry around the doped ions would render their radiative transition probabilities.[24, 25] Besides electric field, the elastic strain is an alternative way for tuning lanthanide doped phosphors. Single-crystal relaxor ferroelectric $(PbMg_{1/3}Nb_{1/3}O_3)_{0.7}$-$(PbTiO_3)_{0.3}$ (PMN-PT) endowed with giant piezoelectric strain has been intensively selected for the investigation of strain engineering.[26, 27] Upconversion PL of BTO: Yb/Er thin films grown on PMN-PT substrates was dynamically tuned, which confirms the PL tunability activated by the PMN-PT based piezoelectric actuators.[17] To date, PMN-PT crystals provide almost the largest interface stress currently available as piezoelectric substrates. However, the delivered strain fields originated from PMN-PT can only reach about 0.4% exerting an influence on the grown films, which corresponds to the PL tunability of 25% and 21% for green and red emission bands of BTO: Yb/Er thin films, respectively.[28]

Larger strains promise larger tunability of the PL emissions on demand. In order to achieve larger interface stress, several lattice-mismatched substrates were employed to induce giant biaxial strain on the as-grown lanthanide doped thin films. In these studies, BTO was selected as the prototypical ferroelectric host material for investigating crystal structure transformation under mechanical stress.[16, 28, 29] Specifically, BTO has moderate lattice mismatch with kinds of commonly used oxide substrates, such as $LaAlO_3$ (LAO), $(La,Sr)(Al,Ta)O_3$ (LSAT), $SrTiO_3$ (STO), PMN-PT, and MgO, which provide an opportunity to investigate the interplay between the upconversion emission

and the crystal filed distortion in a wider range. Previous studies have demonstrated that the dopant ions in the host lattice can be regarded as a spectroscopic probe for crystal structure deformation. Herein, we perform the identifications of the lattice distortion and the crystalline orientation of the single-crystal thin films, and measure the associated luminescent properties.

2. Experiment

Ti-site substitution Er^{3+} doped BTO target with a chemical formula $BaTi_{0.99}Er_{0.01}O_{3-\delta}$ (BTO: Er) was prepared by a standard solid state reaction method.[29] Single-crystal (001) LAO (a=3.792 Å), (001) LSAT (a=3.868 Å), (001) STO (a=3.905 Å), (001) PMN-PT (a=4.024 Å), and (001) MgO (a=4.216 Å) were employed as the lattice-mismatched substrates. The BTO: Er thin films were deposited by pulsed laser deposition (PLD) using the following growth conditions:[28] a coherent KrF laser (248 nm) with pulse energy of 100 mJ (energy density ~ 1.25 J cm^{-2}), repetition rate of 2 Hz; growth temperature of 700 ^{o}C, O_2 pressure of 10 Pa. After the deposition, all the samples were cooled down to 580 ^{o}C in 200 mbar O_2 and maintained at this temperature and atmosphere for 30 min before being cooled down to room temperature. The thickness of the as-grown thin films were measured around 30 nm by the ellipsometer results. The ellipsometric angles Ψ and Δ were measured at room temperature in the 400-800 nm spectral range with a step size of 0.3 nm. Measurements were performed in a reflection mode at an incident angle of 64.91^{o}. The accuracy of the ellipsometry spectroscopic measurement is ± 0.5 Å. The crystal structure characterization was

performed with a Bruker D8 Advance X-ray diffractometer (using Cu K-α_1 radiation, λ=1.5406 Å). The PL spectra were recorded using a SpectraPro 300i spectrophotometer under the excitation of a 980 nm diode laser. All measurements were performed under ambient conditions at room temperature.

3. Results and discussion

Figure 1a shows the θ-2θ spectrum of the BTO: Er films grown on different substrates. Besides the substrates peaks [LAO (002), LSAT (002), STO (002), PMN-PT (002), MgO (002)], no other peaks of the secondary impurities were observed, indicating that the Er^{3+} ions were effectively doped into the BTO host. From the position of BTO: Er peaks, the out-of-plane lattice parameter c and the strain ε_{zz} can be calculated by $\varepsilon_{zz}=(c_{film}-c_{bulk})/c_{bulk}$. Due to the small lattice mismatch, there are strong overlaps of (002) peaks for BTO: Er film with (002) PMN-PT substrate. The BTO: Er (002) reflection peaks on PMN-PT substrates were obtained by subtracting the Ka2 peaks of the substrates. The bulk BTO possesses a tetragonal structure (*P4mm*) with a lattice parameter a=3.992 Å and c=4.036 Å. Considering the bulk lattice mismatch between the film and substrates, c-axis oriented (i.e. c-axis perpendicular to the substrate surface) BTO: Er films on LAO, LSAT, and STO substrates are under in-plane compressive strain, while those on PMN-PT, and MgO substrates should be under in-plane tensile strain. Theoretically, with substrates' lattice constant decreasing, the out-of-plane lattice constant of BTO: Er films will increase. Hence, the BTO: Er diffraction peaks will shift toward lower degree. The in-plane misfit strain ε_{xx} could also be derived by using the

Poisson relation $v = 1/(1-2\varepsilon_{xx}/\varepsilon_{zz})$ with $v = 0.35$.[30] The lattice constant a_{sub} of the substrates, the calculated lattice parameters of the films, and the strain value in BTO: Er films are listed in Table 1. As seen from Table 1, BTO: Er films grown on MgO, PMN-PT, and STO substrates follow the prediction, where the *c* values are increased from 4.002 Å to 4.110 Å, showing the BTO: Er films are *c*-axis oriented. For BTO: Er/LSAT, even though a_{sub} of LSAT is smaller than that of STO, the measured c_{film} (4.066 Å) of BTO: Er thin film is at the intermediate region of the lattice constants from BTO: Er/STO and bulk BTO, indicating the co-existence of *c*-axis to *a*-axis orientation. The broad and asymmetric XRD peak profile of BTO: Er/LSAT is in favor of this hypothesis. The ultimate transformation from *c*-axis to *a*-axis was observed in BTO: Er/LAO thin film. The a_{sub} of LAO is only 3.789 Å, while the c_{film} of above BTO: Er thin film is further down to 4.028 Å, which could be fully *a*-axis grown film. The symmetric XRD peak confirms the unidirectional orientation growth.

In order to understand crystalline orientation and lattice distortion of the films, the strain relaxation process as well as the misfit dislocation formation should be taken into account, which are strongly associated with the estimated in-plane strain ε^0_{xx} [$\varepsilon^0_{xx}(\%) = (a_{sub}-a_{film})/a_{film} \times 100\%$, where a_{film} and a_{sub} are the bulk lattice parameter for thin film and substrate, respectively]. For small lattice mismatch, the strain tends to release gradually across the film by lattice distortion.[31, 32] With lattice mismatch increasing, dislocations, such as threading dislocations will be formed near the interface to relax the strain, instead of lattice distortions.[33] For larger strain, more dislocations will be formed near the interface, resulting in the generation of a polycrystalline film with

different orientations. For the BTO: Er thin film grown on the STO substrate, with a small in-plane compressive strain (-2.18%), the strain is relaxed across the films by lattice distortion. The lattice constant $a \sim 3.924$ Å is almost the same as that of the STO substrate (a=3.905 Å), while lattice constant c is greatly elongated to 4.110 Å. As a result, the c/a ratio for BTO: Er/STO is enhanced to 1.0474. With increasing the in-plane compressive strains (LSAT: ~-3.11%, LAO: -5.09%), the moderate compressive stress is preferred to relax by inserting misfit dislocations near the interface, resulting in a c-axis to a-axis orientation transition. Thus, smaller c/a ratios of 1.0257 and 1.0073 are calculated for LSAT and LAO, respectively. For the BTO: Er film grown on the PMN-PT substrate, the in-plane tensile strain is up to 0.80%. A decreased c value of 4.016 Å and an elongated a value of 4.010 Å are obtained. We can conclude that the tetragonality in BTO: Er film almost vanishes, which leads to a quasi-cubic structure with the c/a ratio down to 1.0015. For the thin film grown on MgO substrate, with an in-plane tensile strain of 5.61%, it gives rise to a significantly reduced c value (~4.002 Å) and an increased a value (~4.023 Å). Thus, the in-plane oriented tetragonal structure appears, with an a/c ratio of 1.009. The calculated c/a ratio, the lattice constant c from XRD θ-2θ scan, and the lattice constant a from Poisson relation calculation as a function of substrates parameter are shown in Figure 2. It should also be noted that for BTO: Er films grown on larger lattice mismatched substrates (LAO, LSAT, and MgO), the obtained in-plane strain values are considerably smaller than the estimated misfit strain ε^0_{xx}. It is consistent with the previously established strain relaxation mechanism in BTO films,[33] also indicating that larger lattice mismatch tends to relax by forming

the misfit dislocation near the interface.

Figure 3 shows the upconversion PL spectra of BTO: Er films on different substrates. The PL spectra consist of two strong green emission bands at 525/551 nm and a weak red emission band at 668 nm, corresponding to the infra $4f^2H_{11/2}/^4S_{2/3}\rightarrow{}^4I_{15/2}$ transitions and $^4F_{9/2}\rightarrow{}^4I_{15/2}$ transition of the Er^{3+} ions, respectively. It is noticed that the emission intensity reaches a maximum value in the film grown on STO substrate, while the minimum value is observed in the film grown on PMN-PT substrate. The results can be classified according to the PL intensities, i.e. BTO: Er/STO > BTO: Er/LSAT > BTO: Er/LAO > BTO: Er/MgO > BTO: Er/PMN-PT. Figure 4 indicates that the arrangement of the PL intensity is consistent with the order of the *c*/*a* ratios of BTO: Er films grown on different substrates. Considering identical growth conditions and thickness of the films, the remarkable distinction of the PL mainly originates from the lattice strain induced structure distortion. In principle, a lower symmetry around the Er^{3+} ions derive a crystal field containing more uneven components into the 4*f* configurational levels and subsequently give rise to the enhanced transitions of lanthanide ions. Figure 5 shows the enhancement factors for green (525 nm/551 nm) and red (668 nm) emission bands as a function of the *c*/*a* ratio. Because BTO: Er thin film grown on PMN-PT has a quasi-cubic structure (*c*/*a*=1.0015), we used the PL intensity of BTO: Er/PMN-PT as the benchmark. It can be seen that the enhancement factors for the green (525 nm/551 nm) and red (668 nm) emission bands of BTO: Er/STO (corresponding to the in-plane strain of ~1.7%) can be up to ~6.5 and 7.1, respectively, which is significantly enhanced compared with our previously reported values obtained from PMN-PT actuators.[17] For

further confirming our hypothesis, we also measured the lifetime at the wavelength of 551 nm corresponding to the $^4S_{2/3} \rightarrow {}^4I_{15/2}$ transition for all the samples. The lifetimes were measured to be 20.8 μs, 23.3 μs, 87 μs, 109.6 μs and 132.6 μs, respectively for the BTO: Er thin films grown on STO, LSAT, LAO, MgO and PMN-PT substrates. It can be found that the lifetime values decrease when increasing the *c*/*a* ratios of BTO: Er films. Together with the enhanced PL intensities, smaller lifetimes indicate increased radiative transition probabilities existed in the BTO: Er thin films with larger *c*/*a* ratios. These results exhibit the prospects of strain engineering on lanthanide doped phosphors. It is intriguing that the arrangement of enhancement factors follows the changing trend of *c/a* ratios, rather along the estimated in-plane strain ε^0_{xx}. Therefore, lanthanide ions can be used as the spectroscopic probe for monitoring *in-situ* stress and strain situations.

4. Conclusions

In summary, biaxial strain induced strong enhancements of upconversion emission were observed in the BTO: Er thin films grown on different lattice-mismatched substrates. The observed remarkable enhancements can be ascribed to the increase in radiative transition probabilities resulting from strain-mediated asymmetry changes at the Er^{3+} ion sites. The quantitative determination of lattice distortion and crystalline orientation is in favor of the observed PL enhancement, which will aid further understanding the interplay between the crystal field and luminescence of lanthanide ions. Our finding not only offers an effective way to improve the luminous efficiency of lanthanide doped luminescent films, but also provides a feasible approach to explore the intrinsic state of

stress and strain in ferroelectric materials.

Acknowledgments

This work was supported by the National Natural Science Foundation of China (No. 61604100, 11404029, 51572033, 11874230 and 51172208), the National Key Research and Development Program (2018YFB0504400), the Fund of State Key Laboratory of Information Photonics and Optical Communications (BUPT), Natural Science Foundation of Tianjin (18JCYBJC41500), RGC GRF (No. PolyU 153281/16P), and the Fundamental Research Funds for the Central Universities.

1. J.-C. G. Bünzli and S. V. Eliseeva, 2013, *Chem. Sci.*, **4**, 1939-1949.
2. G. X. Bai, M. K. Tsang and J. H. Hao, 2015, *Adv. Opt. Mater.*, **3**, 431-462.
3. G. X. Bai, M. K. Tsang and J. H. Hao, 2016, *Adv. Funct. Mater.*, **26**, 6330-6350.
4. W. Zheng, S. Y. Zhou, J. Xu, Y. S. Liu, P. Huang, Y. Liu and X. Y. Chen, 2016, *Adv Sci*, **3**, 1600197.
5. F. Wang and X. Liu, 2014, *Acc. Chem. Res.*, **47**, 1378-1385.
6. Z. P. Wu, G. X. Bai, Y. Y. Qu, D. Y. Guo, L. H. Li, P. G. Li, J. H. Hao and W. H. Tang, 2016, *Appl Phys Lett*, **108**, 211903.
7. M. Shang, C. Li and J. Lin, 2014, *Chem. Soc. Rev.*, **43**, 1372-1386.
8. F. Li, X. Wang, Z. Xia, C. Pan and Q. Liu, 2017, *Adv. Funct. Mater.*, **27**, 1700051.
9. X. Teng, Y. Zhu, W. Wei, S. Wang, J. Huang, R. Naccache, W. Hu, A. I. Y. Tok, Y. Han, Q. Zhang, Q. Fan, W. Huang, J. A. Capobianco and L. Huang, 2012, *JACS*, **134**, 8340-8343.
10. Z. P. Wu, G. X. Bai, Q. R. Hu, D. Y. Guo, C. L. Sun, L. Y. Ji, M. Lei, L. H. Li, P. G. Li, J. H. Hao and W. H. Tang, 2015, *Appl Phys Lett*, **106**, 171910.
11. F. Wang and X. Liu, 2008, *J. Am. Chem. Soc.*, **130**, 5642-5643.
12. Y. Zhang, W. Jie, P. Chen, W. Liu and J. Hao, 2018, *Adv. Mater.*, **30**, 1707007.
13. Y. Zhang and J. Hao, 2013, *J. Mater. Chem. C*, **1**, 5607.
14. W. Z. Wu and Z. L. Wang, 2016, *Nat. Rev. Mater.*, **1**, 16031.
15. X. Wang, D. Peng, B. Huang, C. Pan and Z. L. Wang, 2019, *Nano Energy*, **55**, 389-400.
16. J. Hao, Y. Zhang and X. Wei, 2011, *Angew. Chem. Int. Ed.*, **50**, 6876-6880.
17. Y. Zhang, G. Gao, H. L. Chan, J. Dai, Y. Wang and J. Hao, 2012, *Adv. Mater.*, **24**, 1729-1735.
18. L. X. Zhang, J. Chen, L. L. Fan, O. Dieguez, J. L. Cao, Z. Pan, Y. L. Wang, J. G. Wang, M. Kim, S. Q. Deng, J. O. Wang, H. H. Wang, J. X. Deng, R. B. Yu, J. F. Scott and X. R. Xing, 2018, *Science*, **361**, 494-497.
19. J. Hao and C.-N. Xu, 2018, *MRS Bulletin*, **43**, 965-969.
20. R. Bao, Y. Hu, Q. Yang and C. Pan, 2018, *MRS Bulletin*, **43**, 952-958.
21. G. Ding, F. Gao, G. Wu and D. Bao, 2011, *J. Appl. Phys.*, **109**, 123101.
22. P. Du, L. Luo, W. Li, Y. Zhang and H. Chen, 2013, *J. Alloys Compd.*, **551**, 219-223.
23. H. L. Sun, X. Wu, T. H. Chung and K. W. Kwok, 2016, *Sci. Rep.*, **6**, 28677.
24. M. Zheng, H. Sun, M. K. Chan and K. W. Kwok, 2019, *Nano Energy*, **55**, 22-28.
25. H. Zou, D. Peng, G. Wu, X. Wang, D. Bao, J. Li, Y. Li and X. Yao, 2013, *J. Appl. Phys.*, **114**, 073103.
26. Z. L. Wang, 2010, *Nano Today*, **5**, 540-552.
27. F. Wang, D. Liu, Z. Chen, Z. Duan, Y. Zhang, D. Sun, X. Zhao, W. Shi, R. Zheng and H. Luo, 2017, *J. Mater. Chem. C*, **5**, 9115-9120.
28. Z. P. Wu, Y. Zhang, G. X. Bai, W. H. Tang, J. Gao and J. H. Hao, 2014, *Opt. Express*, **22**, 29014.
29. Y. Zhang, J. H. Hao, C. L. Mak and X. H. Wei, 2011, *Opt. Express*, **19**, 1824-1829.

30. G. N. Greaves, A. L. Greer, R. S. Lakes and T. Rouxel, 2011, *Nat. Mater.*, **10**, 823-837.
31. T. Zhao, F. Chen, H. B. Lu, G. Z. Yang and Z. H. Chen, 2000, *J. Appl. Phys.*, **87**, 7442-7447.
32. C. L. Canedy, H. Li, S. P. Alpay, L. Salamanca-Riba, A. L. Roytburd and R. Ramesh, 2000, *Applied Physics Letters*, **77**, 1695-1697.
33. G. Catalan, B. Noheda, J. McAneney, L. J. Sinnamon and J. M. Gregg, 2005, *Phys. Rev. B*, **72**, 020102.

Table Caption:

Table 1: Lattice parameters of the substrates a_{sub}, out-of-plane lattice parameter of BTO: Er c_{film} from XRD, out-of-plane misfit strain ε_{zz}, in-plane misfit strain ε_{xx}, estimated in-plane misfit strain ε^{0}_{xx}, calculated in-plane lattice parameter a_{film}, and the c/a ratio for BTO: Er films grown on different substrates.

Table 1

substrates	a_{sub} (Å)	c_{film} (Å)	ε_{zz} (%)	ε_{xx} (%)	estimated ε^{0}_{xx} (%)	a_{film} (Å)	c/a
LAO	3.789	4.028	-0.20	0.18	-5.09	3.999	1.0073
LSAT	3.868	4.066	0.74	-0.69	-3.11	3.964	1.0257
STO	3.905	4.110	1.83	-1.7	-2.18	3.924	1.0474
PMN-PT	4.024	4.016	-0.50	0.46	0.80	4.010	1.0015
MgO	4.216	4.002	-0.84	0.78	5.61	4.023	1.0052

Figure Caption:

Figure 1. XRD θ-2θ scan of Er^{3+} doped $BaTiO_3$ films on LAO, LSAT, STO, PMN-PT, and MgO substrates in the 40°–50° range. Dashed lines represent the positions of the characteristic bulk $BaTiO_3$ (002) and (200) reflections.

Figure 2. The *c*/*a* ratio (top), lattice constant *c* and *a* (bottom) of BTO: Er films as a function of the substrates lattice constants.

Figure 3. The upconversion emission spectra of the BTO: Er films grown on LAO, LSAT, STO, PMN-PT, and MgO substrates.

Figure 4. The upconversion PL emission intensity ratio of green-to-red emission (I_{551} nm/I_{668} nm) (top) and the PL emission intensities for green and red emission bands (bottom), as a function of the *c*/*a* ratio for BTO: Er films.

Figure 5. The enhancement factors for red (525 nm/551 nm) and green (668 nm) emission bands as a function of the *c*/*a* ratio for BTO: Er films.

Figure 1

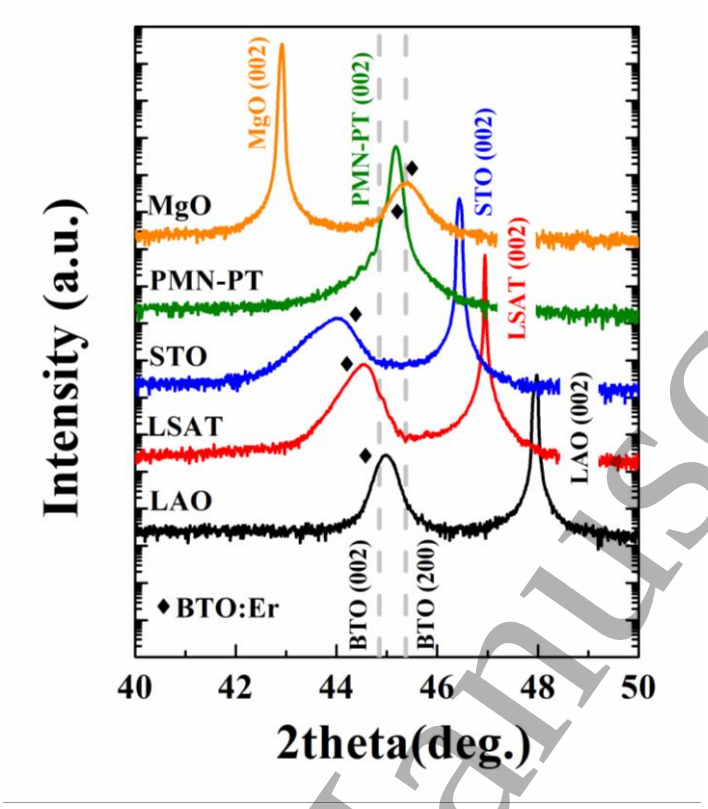

Figure 2

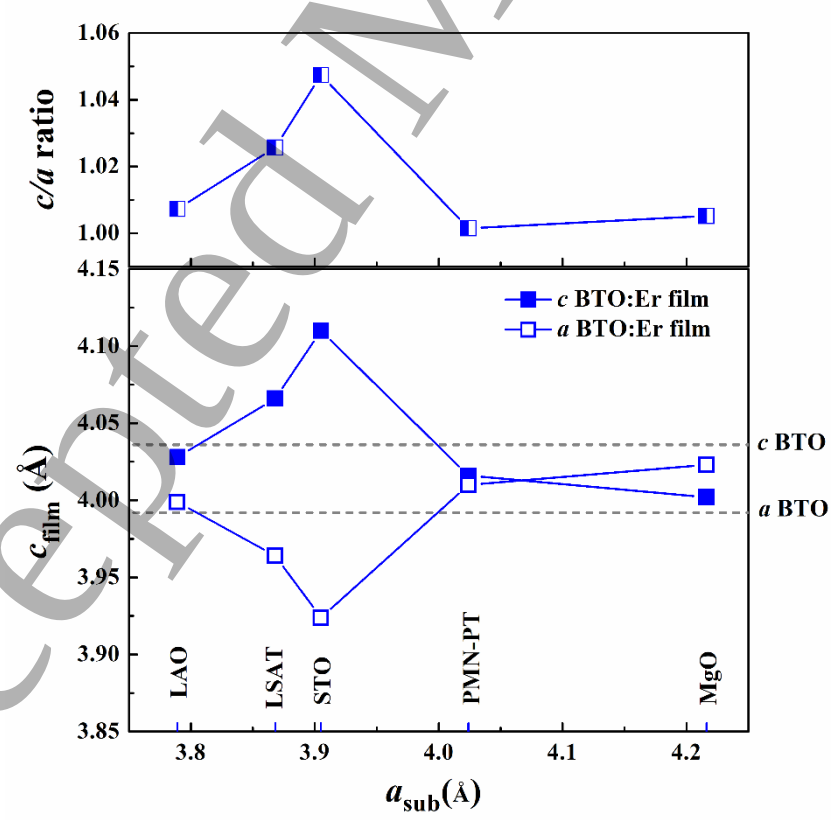

Figure 3

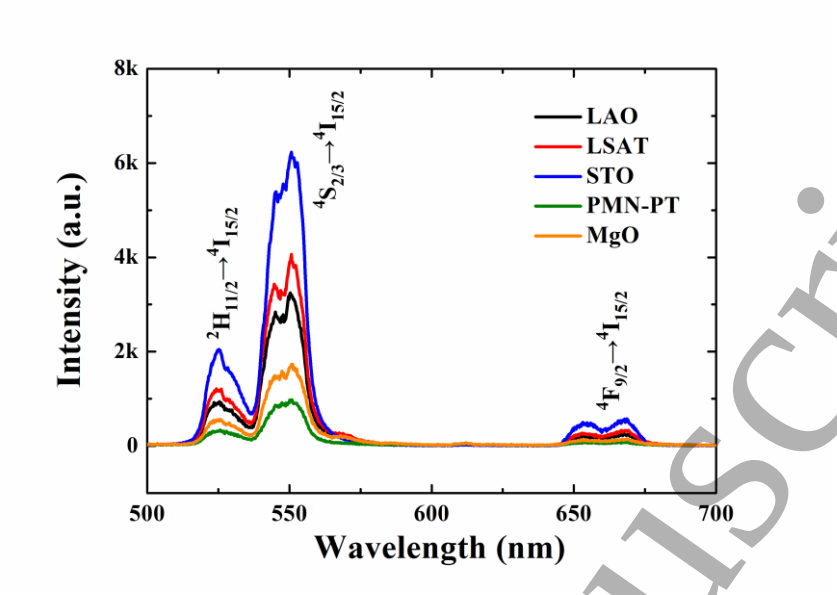

Figure 4

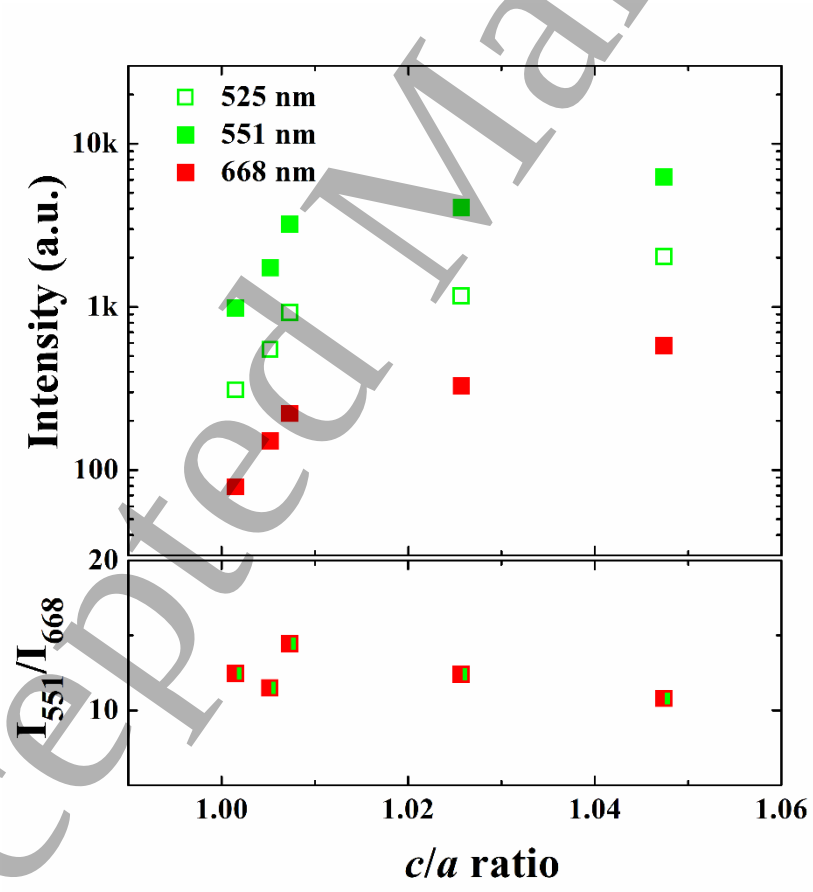

Figure 5